Transitions in the morphology and critical stresses of gliding dislocations in multiprincipal element alloys

Lauren T. W. Fey, Shuozhi Xu, Yanqing Su, Abigail Hunter, and Irene J. Beyerlein

Phys. Rev. Materials **6**, 013605 — Published 7 January 2022

DOI: 10.1103/PhysRevMaterials.6.013605

Transitions in the morphology and critical stresses of gliding dislocations in multi-principal element alloys

Lauren T.W. Fey,[1,2,*] Shuozhi Xu,[3] Yanqing Su,[4] Abigail Hunter,[2] and Irene J. Beyerlein[1,3]

[1]*Materials Department, University of California, Santa Barbara, Santa Barbara, CA*

[2]*X Computational Physics Division, Los Alamos National Laboratory, Los Alamos, NM*

[3]*Department of Mechanical Engineering, University of California, Santa Barbara, Santa Barbara, CA*

[4]*Department of Mechanical and Aerospace Engineering, Utah State University, Logan, UT*

(Dated: December 23, 2021)

Abstract

Refractory multi-principal element alloys (MPEAs) are promising material candidates for high-temperature, high-strength applications. However, their deformation mechanisms, particularly at the dislocation-scale, are unusual compared to those of conventional alloys, making it challenging to understand the origin of their high strength. Here, using an atomistically informed phase-field dislocation dynamics model, we study transitions in the morphology and critical stresses of long gliding screw dislocations over extended distances in a refractory MPEA. The model MPEA crystal accounts for the atomic-scale fluctuations in chemical composition across the glide planes via spatially correlated lattice energies and for the differences in glide resistances between screw and edge dislocations of unit length. We show that the dislocation moves in a stop/start motion, alternating between wavy morphology in free flight and nearly recovered straight screw orientation in full arrest. The periods of wavy glide are due to variable kink-pair formation and migration rates along the length, where portions with higher rates glide more quickly. The critical stress to initiate motion corresponds to the stress required to form and migrate a kink-pair at the weakest region along the length of the dislocation. Heterogeneity in lattice energy leads to variability in the local stress-strain response and to a strain hardening-like response, in which the critical stress to re-activate glide increases with glide distance. Statistical assessment of hundreds of realizations of dislocations indicates that the amount of hardening directly scales with the dispersion in underlying lattice energy.

I. INTRODUCTION

Multi-principal element alloys (MPEAs), comprised of nearly equal fractions of three or more metallic elements, exhibit superior strengths, reaching values far outweighing a weighted fraction of the strengths of the constituent elements. Gaining special interest for harnessing these high strengths in high temperatures are refractory MPEAs, which are a subset of MPEAs that are composed primarily of refractory elements and form a chemically disordered body-centered cubic (BCC) solid solution [1–4]. The strength of a metal is closely linked to the critical stress to move a dislocation through the lattice. Several computational

* laurenfey@ucsb.edu

methods, ranging from atomistic simulation to continuum based dislocation dynamics simulation have been employed to calculate this fundamental critical stress in MPEAs [5–7], and although the approaches and measures used among them vary, they consistently report that moving a dislocation in an MPEA is harder than in the pure refractory metal. However, identifying the origin of strengthening based on a single moving dislocation is not straightforward due to their complex interactions with other dislocations and defects and, especially in MPEAs, peculiarities in the active dislocation mechanisms [8].

Atomic-scale simulation and experimental studies have shown that dislocations in MPEAs behave differently than in pure refractory metals or conventional, dilute refractory alloys [9, 10]. Due to the atomic-scale fluctuations in chemical composition in the glide planes of the dislocations, the critical stress is no longer deterministic and scale invariant, but depends on the length and location of the dislocation [11]. Atomic-scale simulations have shown that the local chemical changes result in a variable dislocation core structure along its line, causing the Peierls (lattice friction) stress for dislocation glide to concomitantly change along the dislocation line [5, 12–16]. As an analogous measure to the Peierls stress for pure metals, atomistic calculations were carried out on a short unit segment ($3b$–$4b$ in length) to define the local slip resistance (LSRs) in a ternary MPEA MoNbTi [17]. The LSRs varied substantially with a 60% coefficient of variation among dislocations in different locations in the material.

Simulations of longer dislocations using atomistic or mesoscale dislocation dynamics methods have shown that mechanisms for dislocation glide are also unusual [9, 11]. In pure BCC metals, the edge-character dislocations move easily compared to the screw-character ones, where the screw-to-edge ratio in critical stress ranges from 10^2 to 10^3 [18–20]. Screw dislocations move by the formation and migration of kink-pairs, straightening after every kink-pair event and lying in wait for the next kink-pair event to occur [21–23]. Long ($> 100b$) straight screw dislocations are often seen in post mortem microscopy of deformed BCC metals [23, 24]. In contrast, compared to dislocations in conventional metals, the dislocation motion seen in molecular dynamics (MD), mesoscale dislocation simulations or in-situ or ex-situ microscopy studies for a wide range of MPEAs, has been variously called wavy, tortuous, or jerky and for both edge and screw dislocations alike [5, 9, 11, 12, 25–27]. Dislocation waviness is generally understood to be a consequence of the variation in local lattice distortion, bond strengths, and dislocation core structure due to the atomic-scale variation

in chemical composition. The statistically harder areas for the dislocation to shear serve as local pinning points and the dislocation bows between them, leading to the wavy appearance or pin/depinning jerky glide. Many MD simulation studies also have reported that the parts of a moving screw dislocation will locally cross slip onto other {110} planes, resulting in cross-kink pairs, which can also cause a wavy morphology and jerky motion [5, 14, 28, 29].

Another peculiarity emerging from MD simulations as a characteristic of dislocations in MPEAs is the markedly lower screw-to-edge ratio in critical stress. Values range from 2 to 10, easily an order of magnitude lower than that in pure metals [5, 17, 30]. Both the short segments used in the LSR calculations and the longer segments in the wavy glide calculations find screw-to-edge ratios in this range, indicating that the reduction cannot be attributed to dislocation lengths. As a final oddity worth mentioning, a recent study of the refractory MPEA MoNbTi found that dislocation slip occurred predominantly on the higher-order {123} and {134} planes [27]. This is unexpected, as dislocation glide in pure BCC metals is typically attributed to the lower-order {110} and {112} planes [31, 32]. Apart from the LSR studies on MoNbTi [17, 27], most MD simulations of dislocations in BCC MPEAs studied glide on the {110} plane.

Because of the computational costs, many of these studies simulated a few dislocation samples moving over short distances. While a few instances can be sufficient for gleaning unusual mechanisms, the substantial variability in critical stress makes it challenging to understand relationship of unusual motion and the critical stress without statistically significant data and statistical analysis. Furthermore, due in part to the waviness, no standard method for defining the critical stress has been adopted. Some studies associate the critical stress to the threshold stress to initiate motion or to move a prescribed dislocation length over a prescribed distance. In the case of the LSR calculations, the short segments of the screw dislocations intentionally precluded study of kink-pair formation and migration.

Mesoscale dislocation dynamics methods provide a simulation framework for studying dislocation behavior in crystalline materials. For refractory MPEAs, Peierls-Nabarro (PN) and phase field dislocation dynamics (PFDD) have been used [6, 11, 33]. The PN study considered a general dislocation moving in a plane with variable misfit energies over specified correlation length. The variable misfit energy creates variable Peierls stress, and the greater variation in Peierls stress in an MPEA produced a critical stress for dislocation glide higher than that of the constituent elements [6]. PFDD is an energy-based, mesoscale dislocation

model that can reach the necessary length scales and number of simulations to study complex and statistical dislocation behavior [34, 35]. While atomistic simulations require fitted interatomic potentials for multi-component systems [36], PFDD can directly incorporate data on lattice energies from first principles calculations [37]. PFDD was previously used to study the statistical behavior of a Frank-Read (FR) source on the {110} plane in MoNbTi, a refractory MPEA, importing *ab initio* data on the local variation in lattice energy into the calculation [11]. The variation was so great that to extract the effect of FR source length and local clustering on FR source activation stresses, thousands of realizations were required.

In this work, using PFDD, we study the role of screw-to-edge ratio and lattice energy distribution on the morphological transitions and evolution of the critical stresses to move long screw dislocations in a refractory MPEA. We also calculate the critical stresses to form dislocation loops from screw-oriented FR sources. In constructing the MPEA crystal, we use generalized stacking fault energies of different areas in bulk random equimolar MoNbTi calculated from DFT to take into account the effects of chemical, distortional, and configurational fluctuations on local bonding and lattice energies. Because at the nano-scale on any given atomic glide plane, the elemental distribution cannot be truly uniformly random, we presume some amount of random local clustering without thermodynamic driven pairings. For completeness, calculations treat a range of correlation lengths, in which the extent of the local chemical clustering is short, less than 1 nm, to relatively long, 6 nm. Respecting the statistical nature of the underlying chemistry, hundreds of realizations are performed, each over extended glide distances, hundred times the width of the dislocation core.

We show that under mechanical straining, dislocation motion is described by successive intervals of wavy glide when the dislocation is gliding freely followed by full arrest when the dislocation nearly recovers its screw orientation. This glide mechanism leads to strengthening, in which the critical stress to re-activate motion increases with glide distance. Statistical assessment indicates that the amount of hardening directly scales with the dispersion in the underlying lattice energy distribution, in magnitude and in correlation length. Our analysis explains that motion initiates at the weakest region to form and migrate a kink-pair and stops when the entire region along the dislocation is too strong to initiate and migrate one. Unlike screw dislocation glide within its pure constituents, in the MPEA, the temperature is not responsible for kink-pair formation and the critical resolved stress would not increase with glide. These findings are based on characteristics fundamental to MPEAs and explain

why MPEAs behave differently than their pure constituents.

II. METHODS

A. PFDD Formulation

In PFDD, the order parameter field, $\phi(\mathbf{r})$, is associated with a unit amount of slip by one Burgers vector on a given slip system, where $\mathbf{r} = (x, y, z)$ is position in 3D crystal [34, 38]. The $\phi(\mathbf{r})$ field indicates whether or not a point has been slipped by a perfect dislocation, with $\phi(\mathbf{r}) = 0$ or 1 corresponding to region that is unslipped or slipped by one Burgers vector, respectively. The interface between slipped and unslipped regions, corresponding to fractional values of $\phi(\mathbf{r})$, represents the dislocation line and the width of this interface the extent of the dislocation core.

The total energy density of the system ψ is comprised of three components:

$$\psi(\boldsymbol{\epsilon}, \phi) = \psi_{\text{elas}}(\boldsymbol{\epsilon}, \phi) + \psi_{\text{latt}}(\phi) - \psi_{\text{ext}}(\phi) \tag{1}$$

where $\boldsymbol{\epsilon}$ is the total strain. $\psi_{\text{elas}}(\boldsymbol{\epsilon}, \phi)$ is the elastic strain energy, which in this system results from the elastic strain produced by the dislocation Burgers vector along the dislocation line and elastic interaction among parts of the dislocation line. $\psi_{\text{latt}}(\phi)$ is the lattice energy, the excess energy cost in breaking and reforming of atomic bonds as the slip plane is displaced relative to the adjacent plane. $\psi_{\text{ext}}(\phi)$ is the work done under an externally applied stress. The derivation of each energy term based on $\phi(\mathbf{r})$ has been given elsewhere [35, 38].

The elastic energy density is expressed as

$$\psi_{\text{elas}}(\boldsymbol{\epsilon}, \phi) = \frac{1}{2}(\boldsymbol{\epsilon} - \boldsymbol{\epsilon}^{\text{p}}(\phi)) \cdot \mathbf{C}(\boldsymbol{\epsilon} - \boldsymbol{\epsilon}^{\text{p}}(\phi)) \tag{2}$$

where $\boldsymbol{\epsilon}^{\text{p}}(\phi)$ is the plastic strain. The elastic stiffness tensor $\mathbf{C}$ considers the cubic elastic anisotropy of the material [39].

The lattice energy has been related to the γ surface, the excess potential energy per unit area to displace one half crystal with respect to the other across a plane [40]. For refractory metals, as well as refractory MPEAs, DFT and MD calculations find that the stacking fault energy along the $\langle 111 \rangle$ slip direction for all slip planes can be described reasonably well by $\gamma_{\text{usf}} \sin^2(\pi\phi)$, where γ_{usf} is the peak barrier, referred to as the unstable stacking fault energy (USFE) [41–44].

In PFDD, the lattice energy per unit volume for BCC metals is given by

$$\psi_{\text{latt}}(\phi) = \frac{\gamma_{\text{usf}}(x,y)}{d_z}\beta(\theta)\sin^2(\pi\phi) \tag{3}$$

where d_z is the interplanar spacing. For the (hkl) plane, the interplanar spacing is $d_z = a_0/\sqrt{h^2+k^2+l^2}$, where a_0 is the lattice parameter. The USFE is a function of the position due to the random nature of an MPEA. The scaling function $\beta(\theta)$ accounts for variation in lattice energy with the character of the dislocation, which is identified by the character angle, θ. This is the angle between the dislocation line direction and the Burgers vector, thus, for a screw dislocation, $\theta = 0$ and for an edge dislocation, $\theta = \pi/2$. Due to its non-planar core, a screw dislocation has the highest barrier [45], whereas the edge dislocation, with its planar core, has the lowest. The barriers for mixed dislocations, with both edge and screw components, lie in-between. To reflect these character-dependent core effects, we assume a continuous $\beta(\theta)$ taking on the following form [11],

$$\beta(\theta) = \left(1 - \frac{1}{R}\right)\cos^2\theta + \frac{1}{R}, \tag{4}$$

where $R = \sigma_{\text{screw}}/\sigma_{\text{edge}}$, the ratio of the Peierls stress for screw to edge.

Finally, the work done by the gliding dislocation under the applied load is

$$\psi_{\text{ext}} = \boldsymbol{\sigma}_{\text{app}} \cdot \boldsymbol{\epsilon}^{\text{p}}(\phi) \tag{5}$$

where $\boldsymbol{\sigma}_{\text{app}}$ is the applied stress tensor.

The order parameters evolve towards equilibrium via the Ginzburg-Landau equation:

$$\dot{\phi} = -m_0\partial_\phi\psi \tag{6}$$

where m_0 is the Ginzburg-Landau coefficient. This form neglects thermal noise and the effects of temperature on dislocation drag. Randomness in dislocation motion resulting from temperature will be discussed at the end.

B. Dislocation set up

We simulate dislocation motion in a single crystal that is oriented such that the x and y axes lie in the slip plane and the z axis is aligned with the slip plane normal. The computational grid is orthogonal and the grid points coincide as closely as possible with

the atomic positions [46]. Accordingly, the grid spacings in each direction depend on the slip plane being simulated. Previous work has shown that matching the grid points with the lattice points yields the best agreement with molecular statics (MS) calculations for dislocation cores [47]. Table I summarizes the grid spacings, where d_x and d_y are the spacings within the slip plane and d_z, the interplanar spacing.

To study dislocation loop formation, we insert an FR source on the slip plane, using the method described in previous PFDD models [11, 46]. In all calculations, the length of the source is $20b$ and its Burgers vector is $(a_0/2)[111]$ and its plane lies in the center of the crystal. Both screw-oriented and edge-oriented sources are considered. We employ 3D periodic boundary conditions and a computational grid size of $128 \times 128 \times 128$. This cell size has been shown previously to yield negligible effects of image dislocations present due to the periodic boundary conditions for sources of this length [11, 46]. A shear stress is applied in the slip plane and directed along the Burgers vector. Thus, the plane on which the FR source lies is the maximum resolved shear stress plane (MRSSP). The applied shear stress is raised in increments of 0.001μ (where μ is the isotropic Voigt averaged shear modulus and is equal to 43 GPa) until the source activates, after which it is held constant. At each stress increment, the solution procedure is run until convergence, which is defined as when the norm of the change in order parameters is less than 10^{-5} between successive time steps. For convergence, the quantity $m_0\Delta t$, where Δt is the time step, is set to $0.05\mu^{-1}$.

To study long dislocation propagation, a screw-dislocation dipole with $(a_0/2)[111]$ Burgers vector is inserted onto the slip plane lying in the center of the crystal. The simulation cell dimensions are $256 \times 128 \times 128$, and periodic boundary conditions are employed in all three directions. The length in x is doubled to extend the distance the dislocations can glide. The dislocation is 128 b long within the periodic cell, and the dipole separation is 64 grid points in the x direction. A symmetrical USFE surface mirrored over the line $x = 128$ is used such that the two parallel dislocations experience identical USFE landscapes during glide. The applied shear stress is aligned with the plane of the dislocation and in the direction of its Burgers vector, making the plane of the dislocation the MRSSP. Application of the stress and solution procedure are the same as described previously for loop formation.

C. MPEA MoNbTi properties

For the MPEA, we need the elastic moduli tensor $\mathbf{C}$ and lattice parameter a_0 for the bulk material, the spatial distribution of $\psi_{\text{latt}}(\phi)(x, y)$, and the ratio R between screw to edge dislocations for a given type of slip plane. From DFT calculations, MoNbTi is BCC with $a_0 = 3.225$ Å and exhibits cubic elastic anisotropy with constants $C_{11} = 252.13$ GPa, $C_{12} = 134.11$ GPa, and $C_{44} = 32.41$ GPa [48].

In an MPEA, the $\psi_{\text{latt}}(\phi)(x, y)$ fluctuates in (x, y) over atomic-scale dimensions across a given plane. Here we build several statistical realizations of glide planes over 40 nm in side length that are spatially heterogeneous in lattice resistance and in the extent over which the local lattice resistance prevails. The lattice resistance to shear a plane involves breaking bonds and depends on the strength of the atomic bonds that straddle a particular glide plane. The model MPEA we consider is an ideally random, equi-molar MoNbTi with no local chemical short-range ordering. However, at the scale of an elementary dislocation segment, a few Burgers vectors in length, the composition and configuration of atomic elements and hence lattice distortion varies spatially [49], causing the lattice resistance to fluctuate concomitantly. Obtaining the lattice energy necessarily then calls for atomistic calculations, preferably ones that depend on the electronic structure but nevertheless account for the lattice distortion and chemical composition effects on bonding across the crystallographic plane of interest [50]. Atomistic studies of the solute-dislocation interaction energy in refractory MPEAs have shown that the energy change due to a solute atom near a dislocation is well approximated by the change in USFE due to that solute atom [51, 52].

For the USFE distributions in MoNbTi for the PFDD calculations to follow, we take these values from DFT and MS calculations reported recently for MoNbTi [48]. In brief, the calculations begin with a 3D special quasi-random structure of the MoNbTi. The γ-curves are calculated for a given plane with a cross-sectional area of 30 to $60b^2$, several times wider than the magnitude of the Burgers vector and longer than a complete lattice translation vector. The calculations were repeated for a sampling of 10–30 distinct areas in the volume for each plane type.

With USFE distributions in hand, we need to specify the region over which the local USFE extends. For this, we employ a correlated surface method introduced in Ref. [11] for MPEAs, which builds upon a methodology for generating correlated rough surfaces presented in

Ref. [53]. We refer the reader to these references for details. The method requires continuous USFE distributions for input, for which we choose the Gaussian distribution, which will be described shortly. An important physical length scale of the method is the correlation length l, which represents the extent of the local lattice energy in plane, or specifically, the distance two neighboring regions of distinct lattice energy are correlated more than 10%. The method allows for the lattice energy to vary smoothly in plane, avoiding any artificial modeling of phase boundaries. Since l is unknown but yet an unavoidable consequence of the atomic composition of MPEAs, we repeat calculations for l ranging from $1w_0$ to $20w_0$, where w_0 is the average core width of the dislocation in an average MoNbTi alloy on the {110} plane, $2.15b$ [11]. The l range spans from one-tenth to twice the length of the FR source and approximately one-hundredth to one-fifth the length of the screw dislocation. Thus, any profound influence of l ought to emerge in the simulations to come. Since we do not claim to account for chemical short range ordering (CSRO), the value of l is not associated with a particular chemical composition or temperature-time processing method. But as of late, the CSRO effect could arguably be a critically important factor, a point we will return to in Section IV.

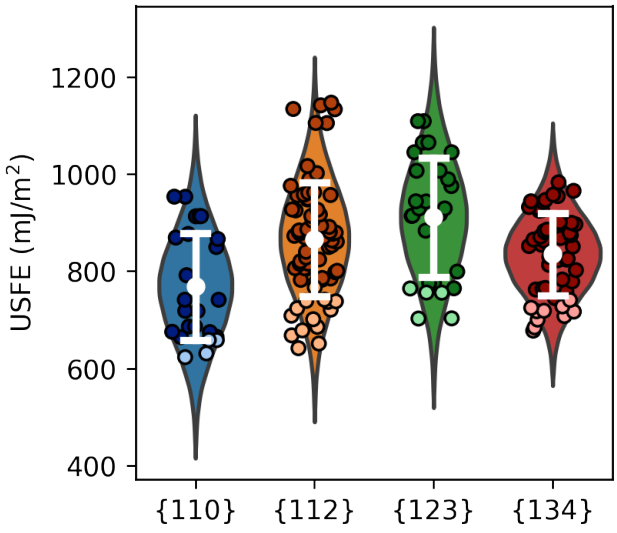

FIG. 1. The USFE values calculated with DFT for each slip plane type and the normal distributions incorporated into the PFDD calculations. The mean and standard deviation for each plane are shown by the white point and error bars, respectively. The lighter colored points represent the bottom 20% of each distribution, where athermal kink-pairs are likely to be nucleated.

To build hundreds of realizations of correlated USFE slip planes for our PFDD simulations, we fit a Gaussian distribution function to each discrete USFE data set provided by atomistic simulation. Figure 1 presents our Gaussian distribution fits along with the discrete USFE distributions. The plane types exhibit USFE distributions distinct in mean and standard deviation, which are summarized in Table I. For a pure metal, the USFE is often used to infer the preferred slip plane for dislocation glide [54, 55]. If we were to use the mean value, the {110} plane is the easiest and the {123} plane the hardest, a ranking not unexpected for a pure metal. Yet, we find that in MoNbTi, the coefficient of variations among these planes are not the same. Since the USFEs are widely distributed and dissimilar, we remark also the lower tails of these distributions, which follow a different ranking, suggesting that these planes are more similar in their weaker regions than the mean value would suggest. The 20% lower quantile, for instance, which is shaded a lighter hue in Figure 1, starts at 775 MPa, 760 MPa, 745 MPa, and 660 MPa, for the {112}, {123}, {134}, and {110} planes, respectively.

Finally we determine an appropriate value for R for each plane based on atomic-scale calculated data of MoNbTi. R is commonly associated with ratio of the Peierls stresses for screw and edge dislocations of unit length. However, in an MPEA, the equivalent stress to the Peierls stress is not independent of length or location as in a pure metal. For this reason, it was called a local slip resistance (LSR) [27]. In prior work, using atomistic simulations, the LSR for a unit screw piece and edge piece less than 1 nm in length were calculated at different regions in a uniformly random volume of MoNbTi [17, 27]. The segment length modeled was intentionally made short so that the dislocation remains straight as it moves along the lattice vector in the plane, as in a classic Peierls stress calculation. Importantly, for the screw dislocation, this length is shorter than the width of a kink pair [45]. For our calculations, R is taken as the ratio of the average screw to edge LSR and the plane-dependent R values are summarized in Table I. All planes have a relatively low R, an emerging commonplace characteristic for MPEAs [5, 10, 12, 56, 57], compared to that for pure metals which is orders of magnitude higher [18, 20, 23, 58]. Among these four planes R still varies by one order of magnitude. The {112} plane represents a very low R plane, with only 1.4 and the {134} plane the highest with 11.8.

Together, the differences in USFE distribution and R among the four planes provides the opportunity to study their effect on dislocation dynamics in the same material. For

each plane, we perform 30 simulations of FR sources and 30 realizations of long dislocation propagation per plane per l.

TABLE I. The parameters used in the PFDD simulation for each plane type. The mean and standard deviation of the USFE are given in mJ/m^2. The screw-edge ratio is unitless. The grid spacings d_x, d_y, and d_z are given in units of the Burgers vector b. d_z is always the interplanar spacing in the slip plane normal direction, and d_y is the spacing in the Burgers vector direction.

	Mean USFE	S.D. USFE	C.O.V USFE	Screw-Edge Ratio	d_x	d_y	d_z
{110}	768	111	14.5%	4.65	1	1	0.8165
{112}	865	118	13.6%	1.40	0.8165	1	0.4714
{123}	911	125	13.7%	6.78	0.8135	1	0.3086
{134}	835	85	10.2%	11.8	0.8498	1	0.2265

III. RESULTS

A. Dislocation Multiplication

We first analyze the effect of USFE distribution and R on operation of a screw-oriented FR source. The applied stress is raised just high enough to operate the dislocation source and then held constant. Figure 2 shows the time sequence of the dislocation line from an activated source typical of each plane. The spatial variation in lattice energy across the plane for these chosen realizations is indicated by the color mapping of local USFE values. On the {110} plane, the most studied plane in pure and MPEA refractory metals, the line morphology of the screw and non-screw parts are wavy. Particularly in the later sequences, the screw portions move slower than the edge portions and the ensuing loops are oblong. The morphology of the line in each time sequence from the source on the {112} plane have similar features, with the developing loops that are noticeably oblong. Similar wavy glide has been seen in MD simulations of other refractory MPEAs and has been a common observation for MPEAs [5, 9, 10, 12, 14]. In all the realizations, like those displayed in Figure 2, each FR source eventually produces a full dislocation loop that glides unhindered out of the simulation cell. In none of the sequences shown does the dislocation loop fully arrest, although the waviness of some or all parts of the dislocation line may suggest otherwise.

The time sequence of the dislocation line for sources on the {123} and {134} planes show different morphologies. While the screw and non-screw portions are wavy, the lines are less tortuous than those on the {110} and {112} planes. Also, in contrast to the other two planes, the loops developing on the {123} and {134} planes have a lower aspect ratio, signifying similar edge and screw mobilities. The smoother glide behavior and nearly equal mobilities are unexpected since these two higher order planes have the highest R. Transitions to smooth glide have been reported to occur at high applied driving stresses [9]. However, here, the applied stresses in the {123} and {134} examples are lower than those in the {110} and {112} examples. While the nearly face-centered cubic (FCC)-like behavior of FR sources on these planes is counter-intuitive, it is worth remarking that in experimental testing of this MPEA, dislocations are seen most often on these two planes in deformed material and less so on the {110} plane [27].

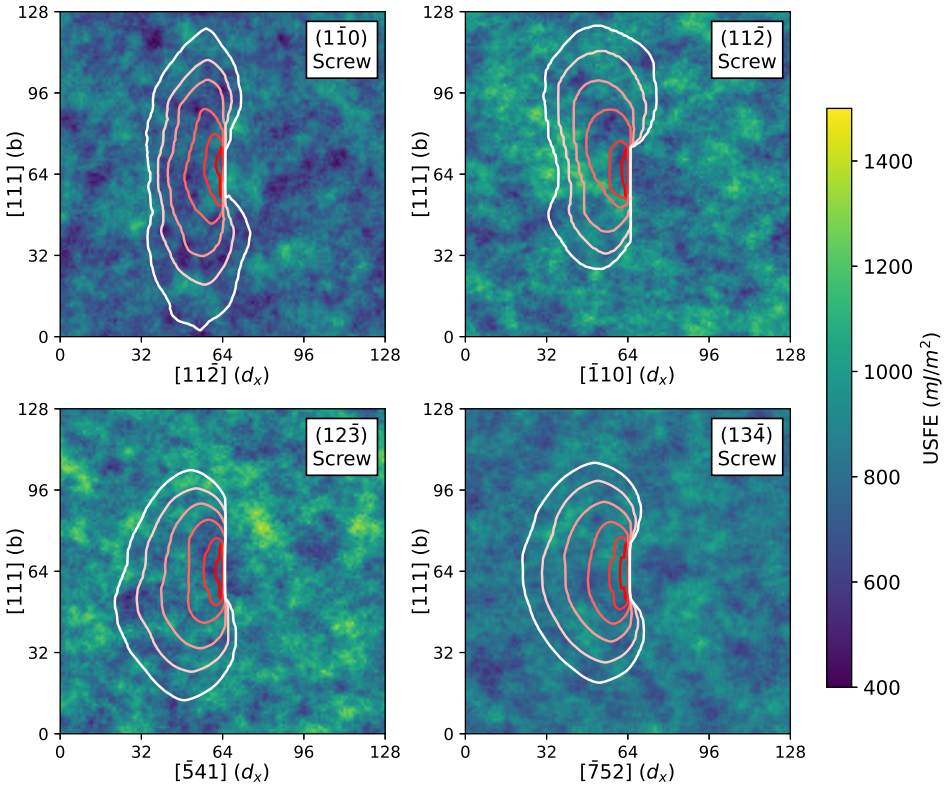

FIG. 2. Representative examples of screw-oriented FR source operation on each of the four planes studied. All surfaces have correlation length l equal to $5w_0$. Dislocation lines are colored with respect to time. Lighter loops indicate a later time step than darker loops.

We identified the critical stress, σ_{FR}, to activate each source. Figure 3 shows values of

σ_{FR} for all 60 realizations for each of the eight l. The variation in σ_{FR} is clearly substantial, calling for a probability distribution that represents well each σ_{FR} distribution for a given l. Our analysis proves the data fit a lognormal distribution in all cases. Comparing the lognormal mean, $\bar{\sigma}_{\mathrm{FR}}$, finds that, on average, the FR sources were hardest to activate on the {112} plane and easiest on the {134} plane. High critical stresses to move dislocations in MPEAs are thought to be related to the variation in lattice energy or the random occurrence of relatively larger local barriers [5, 9]. However, the mean and coefficient of variation (COV) in USFE for the {112} plane are not the highest nor for the {134} plane are they the lowest (see Table I). Further, for no slip plane did l noticeably affect $\bar{\sigma}_{\mathrm{FR}}$.

To determine which properties govern σ_{FR}, we study the dislocation line morphology at the moment σ_{FR} is reached and its relationship to the underlying USFE. In a pure metal, the dislocation line bows out between the two pinned ends, and the critical shear stress at which the line continues to glide unstably corresponds to a critical radius of curvature. In the MPEA, instead of bowing out uniformly, a kink-pair nucleates along the length of the source, and the edge-oriented portions of the kink-pair move along the dislocation line to advance the dislocation. Examples of these kink-pairs on screw-oriented FR sources are shown in the left column of Figure 4. Activation of an FR source includes both kink-pair formation, with the screw protruding normal to the line, and kink-pair migration, with the two edge segments gliding apart. If the shear stress is removed before migration, the straight source is recovered. An activated kink-pair advances the screw portion of the dislocation line forward, into another region of the material, at which point another kink-pair activates. Through successive activation of kink-pairs, the dislocation line bows out. The edge portions having migrated to the pinned ends builds non-screw portions. While in time, the source bows out as in a pure metal (as seen in the early time sequences in Figure 2), it is already in operation when it reaches this configuration in an MPEA.

It is, therefore, observed that the mechanism to activate unstable motion is a kink-pair. The kink-pair triggering event applies to all l and crystallographic planes. Identifying the size of a successful kink-pair is difficult, since by definition, the edge portions of the kink-pair immediately move apart, but it is clear that they are b in height and, when first formed, narrower than the length of the source, being approximately $1b$ to $3b$. More importantly, their size is found uncorrelated with l, in spite of the order-of-magnitude wide range of l. Comparing the first successful kink-pair location with the underlying USFE for all cases

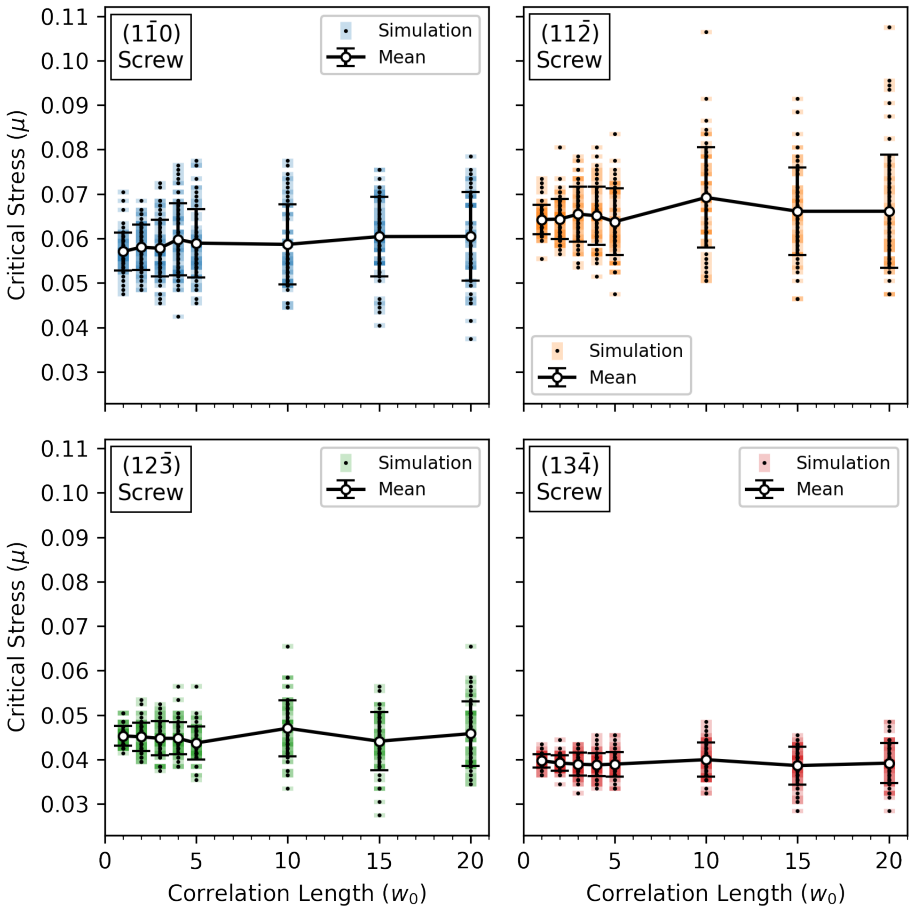

FIG. 3. The critical stresses to activate a screw-oriented FR source on each plane. Each colored box is a separate simulation, and darker colors indicate where multiple simulations give the same critical stress value. The mean for each correlation length is also plotted with error bars corresponding to the standard deviation of the distribution.

finds that the former is strongly correlated with the weakest region along the initial source length. The weakest region means a low barrier to move both the screw and edge parts of the kink-pair. The lower tail of the USFE distribution, which applies to the screw parts, combined with the corresponding R, for the edge parts, and not the mean USFE, decide σ_{FR}. Accordingly, the $\{112\}$ plane has statistically the hardest regions due to its low R, and the $\{134\}$ the weakest regions due to its high R.

Next, we study the effect of the USFE and R on the operation of edge-oriented FR sources of the same length. The initially straight edge segments are not expected to move by kink-pair activation. Figure 5 shows the time sequence of the dislocation lines as these

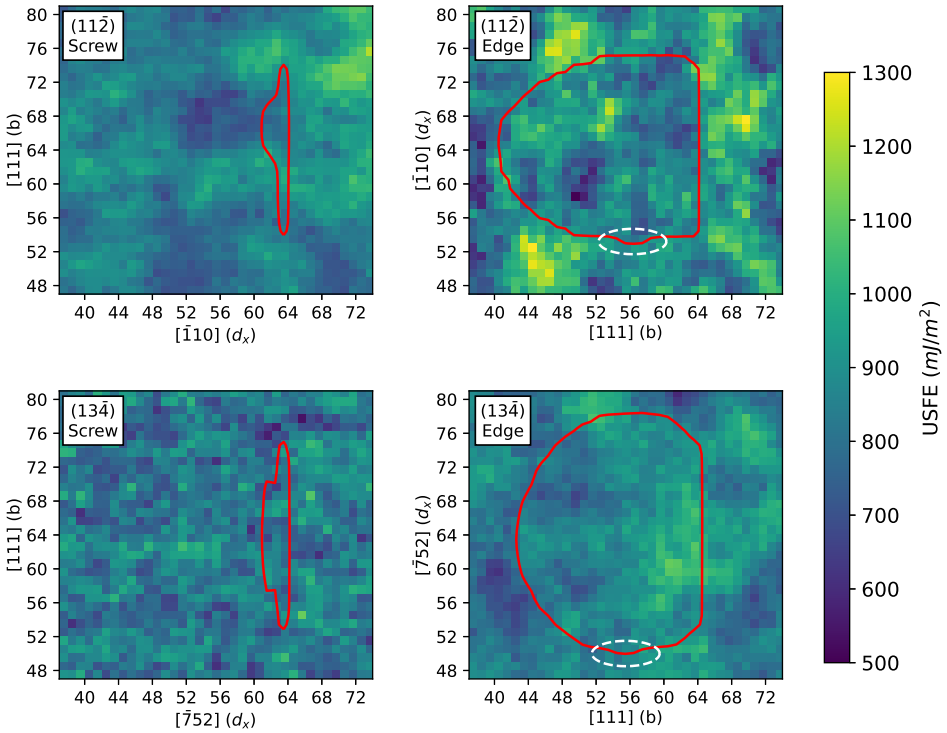

FIG. 4. The critical stages of FR source activation for both a plane with a low screw-edge ratio, {112}-type, and a plane with a high screw-edge ratio, {134}-type. Both screw- and edge-oriented sources show kink-pair nucleation as the limiting step. Before these kink-pairs form, the dislocation will fall back to its original position if the stress is unloaded. The correlation lengths used in these examples range from $1w_0$ to $10w_0$.

sources operate under an applied shear. A typical example is selected for each plane. On the {110} and {112} planes, the lines are wavy and the growing loops are elongated, indicating their two lateral screw portions are moving slower than the edges. On the {123} and {134} planes, a different scenario occurs. The developing loops adopt only slightly wavy lines and the loops expand nearly isotropically. The critical stress distributions σ_{FR} are obtained from the 60 realizations for a given l and slip plane. All data points are presented in Figure 6. Like the screw-oriented sources, the lognormal mean of σ_{FR} for the edge-oriented sources are insensitive to l and indicate that sources are hardest to operate on the {112} plane and easiest on the {134} plane. These similarities suggest that the same mechanism activates edge and screw sources. However, with all else being equal, the edge sources are consistently weaker than the screw sources, and even the ratios of critical stress for screw to edge sources

for all slip planes are similar, ranging from 1.5 to 1.7, and seemingly unaffected by R or the USFE distribution.

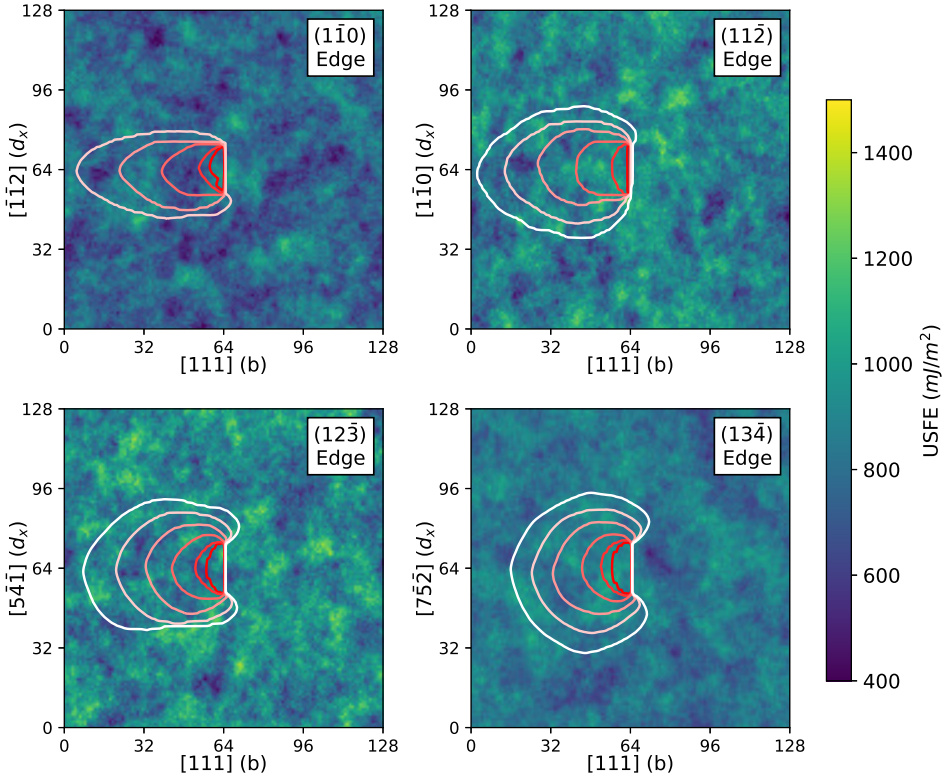

FIG. 5. Representative examples of edge-oriented FR source operation on each of the four planes studied. All surfaces have correlation length l equal to $5w_0$. Dislocation lines are colored with respect to time. Lighter loops indicate a later time step than darker loops.

The line configuration corresponding to σ_{FR} is identified for the edge-oriented sources. Under subcritical stresses, the entire length of the source bows out between the two pinning points, forming two straight screw segments normal to the source. The source becomes critical when the loading state can activate a kink-pair along either of these two screw segments. Otherwise, the bowed-out dislocation recovers its original position when the stress is unloaded. Two examples are shown in the left column of Figure 4. We, therefore, see why σ_{FR} for edge-oriented sources follow the same relationship with the USFE as screw-oriented sources. Both are triggered by forming and migrating a kink-pair in the weakest USFE region along the straight screw portions of the dislocation. The edge cases are consistently about 60% weaker than the screw cases, since the edge-oriented source can sample more of

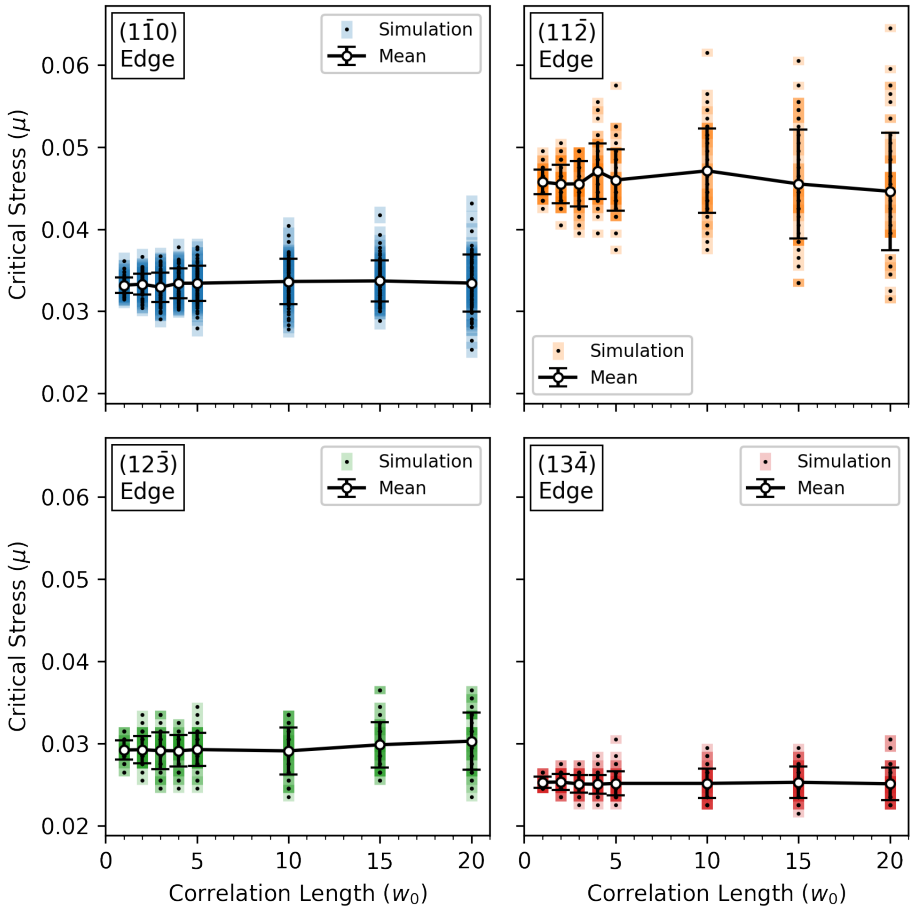

FIG. 6. The critical stresses to activate an edge-oriented FR source on each plane. Each colored box is a separate simulation, and darker colors indicate where multiple simulations give the same critical stress value. The mean for each correlation length is also plotted with error bars corresponding to the standard deviation of the distribution.

the USFE surface by extending the screw dislocation lines.

B. Dislocation Propagation

We next analyze the role of the USFE and R on propagation of a long screw dislocation, $>$ 40 nm in length, which is about 14 times greater than the FR source length. The dislocation is not pinned and can glide freely. Six different l ranging from $1w_0$ to $20w_0$ were studied with 30 distinct samplings from the USFE distributions for each. To determine the threshold stress to move the dislocation across the plane and outside of the simulation cell, the applied

shear stress was slowly incremented until dislocation glide was observed. Figure 7 shows several example stress-strain curves for each plane, all of which are unlike those expected in a pure metal. In a pure metal, the critical stress to move a screw dislocation corresponds to that needed to form and migrate a kink-pair under a given temperature. It is deterministic and unvarying temporally or spatially, apart from the aid from thermal noise. For each glide plane in an MPEA, however, the responses among the different realizations are highly variable; no two are alike. They indicate stop/start motion, wherein the dislocations become pinned and stress increases are required to continue glide. Therefore, these dislocations experience strain hardening. Yet, unlike classic strain hardening, the amount of strain between full stops varies, not necessarily increasing with each rise in stress. These curves terminate at the final stress needed for runaway glide out of the simulation cell. In most cases, the stress to initiate motion, σ_i, is not sufficient to sustain glide across the plane and is lower than the penultimate stress reached in the stress-strain curve, σ_f, which we designated as the stress required for the dislocation to escape the cell.

Due to the substantial variation, we analyze the critical stress results from a statistical viewpoint. Figure 8A compares the distributions for σ_i among the four planes. As would be expected from the few examples in Figure 7, substantial variation in σ_i is seen in all cases. An interesting observation is the persistent consistency in the mean and dispersion in the σ_i distributions in spite of differences in the USFE, l and R. These calculations suggest that average σ_i does not represent well the critical resolved shear stress to start the glide of a screw dislocation, is not sensitive to the spatial variation in lattice energies, and not a discriminating measure of preferred glide plane.

An analysis of σ_f presents markedly different observations. Figure 8B shows the σ_f/σ_i distributions for the same cases. Motion of a screw dislocation on the {110} plane experiences not only the greatest increase in critical stress but also additional enhancements in resistance with l. However, glide on the {134} plane undoubtedly incurs the least strengthening and shows negligible dependence on l. The other two planes exhibit similar, non-negligible hardening propensity, like the {110} plane but to a lesser degree. This significant difference in σ_f/σ_i could explain the experimental observations of gliding dislocations on the {112}, {123}, and {134} planes, but not the {110} planes in this MPEA [27].

To understand the hardening behavior, we study the morphology of the dislocations under the applied shear stress and find that the dislocation line configuration changes in time and

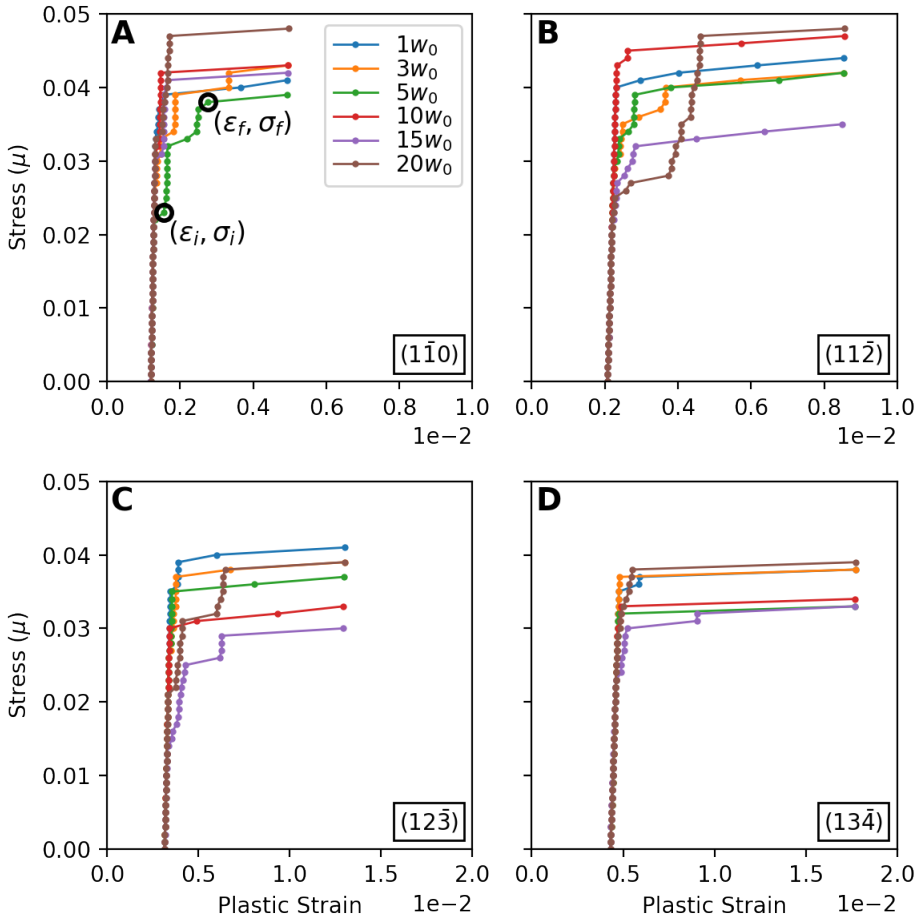

FIG. 7. (A–D) Several stress-strain curves from screw dislocation propagation simulations on each slip plane type. The curves show a characteristic "staircase" as dislocations are pinned and unpinned several times before finally annihilating with periodic images. The definitions of σ_i and σ_f are illustrated in (A).

is wavy during most of the simulation. Figure 9 shows a typical example for each slip plane throughout the full simulation time. In each case, the dislocation remains straight and in its original position under zero stress. When the stress is increased past a critical point, a kink-pair forms at some weak location and migrates some distance, advancing this part of the dislocation by b. Each advancement places that part of the screw dislocation into a new region, with a different random sampling of lattice energies, providing the opportunity to activate more kink-pairs. As the lattice energies vary over the long 40 nm length, when and where kink-pairs activate varies statistically. Under this glide mechanism, different kink-pair activation rates along the same dislocation give it a wavy appearance. Waviness is a common

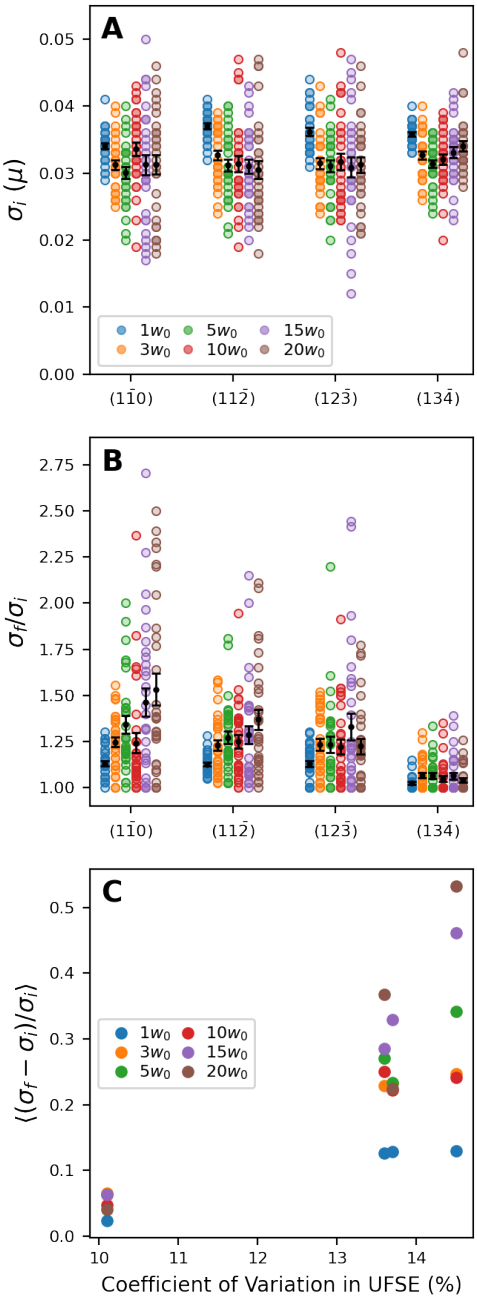

FIG. 8. (A) The distribution of σ_i, the critical stress to initiate glide, grouped by plane type and correlation length. Darker symbols correspond to critical stresses shared by multiple iterations. The black dots show the mean stress for that correlation length and plane, with error bars equal to standard deviation across the 30 iterations. (B) The ratio σ_f/σ_i for each plane as a function of correlation length. This value corresponds to the amount of hardening that occurs during dislocation glide. (C) The quantity $(\sigma_f - \sigma_i)/\sigma_i$ for each correlation length plotted against the coefficient of variation of the underlying USFE surface. Higher variance in USFE leads to more hardening as the dislocation glides.

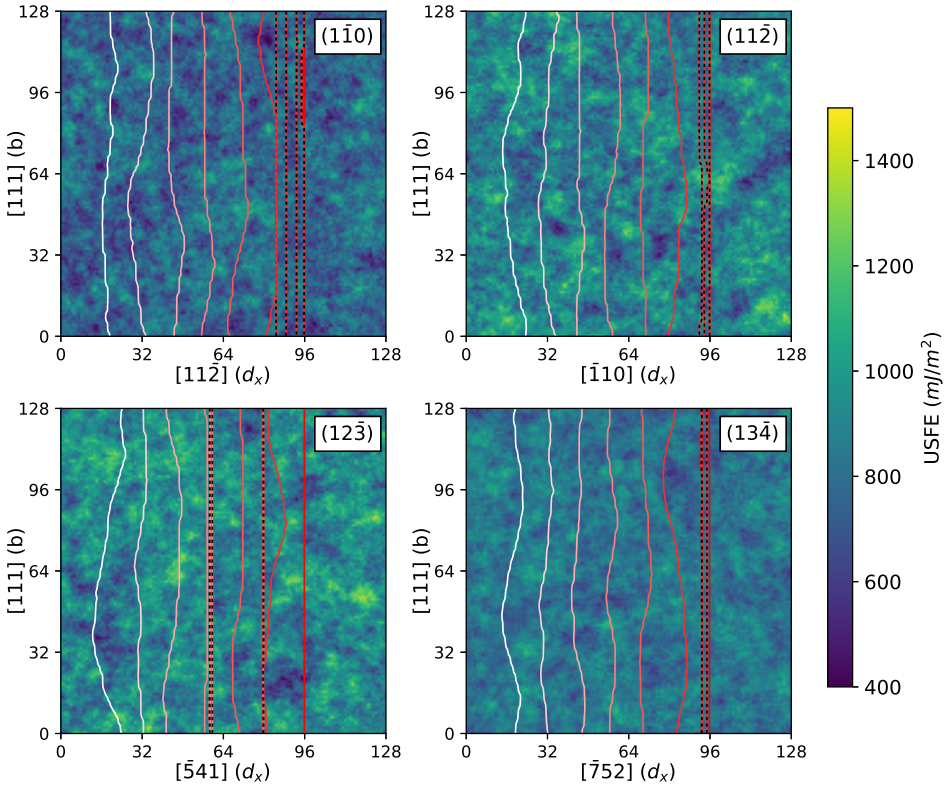

FIG. 9. Representative examples of screw dislocation propagation on each of the four planes studied. The dashed lines indicate stable dislocations under stress, which require an increase in applied stress to advance. All four planes shown have a correlation length of $3w_0$, and dislocation lines are colored with respect to time, where lighter colors indicate a later time step.

observation among MD and other discrete dislocation dynamics simulations of dislocation lines tens of nanometers in length for a wide range of MPEAs [5, 9, 10, 12]. Here, we show that the waviness originates from different parts of the same dislocation forming kink-pairs at different rates and it pertains to all four planes, for all l, and in all realizations, in spite of differences in the underlying USFE distributions, l and R. Only screw-character dislocations move in wavy glide via this mechanism. The waviness alone does not explain the differences in hardening seen in Figure 7 and role of the USFE on σ_f.

To rationalize the USFE effects on strain hardening, dislocation line configurations are analyzed in relation to changes in stress. In all cases, the dislocation glides via a stop/start mechanism. It can be described as alternating intervals of non-stop glide under constant stress and full arrest requiring an increment in stress (Figure 10). The dislocation takes on a wavy morphology as it glides continuously and then becomes nearly straight, close to

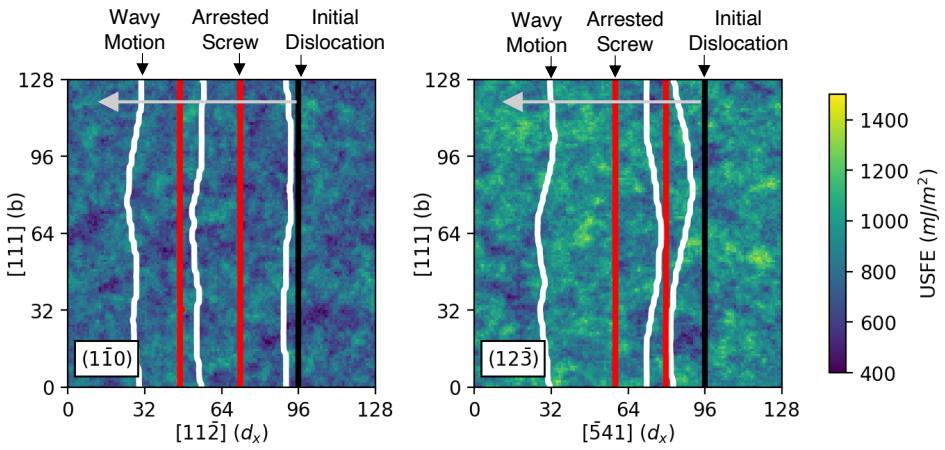

FIG. 10. Representative examples of the progression of screw dislocation glide in MoNbTi. The initially straight screw dislocation (shown in black) appears wavy during glide (shown in white) but become arrested under stress and returns to a straight screw morphology (shown in red). These examples are from a {110}-type plane and {123}-type plane, but dislocation glide proceeds in a similar fashion for all planes studied. The correlation length l is $3w_0$ for both cases.

its original screw orientation, when it completely stops. We find that continuous glide for the entire dislocation is sustained as long as any part of it can activate kink-pairs. The dislocation moves in free flight by statistical kink-pair activation, until it reaches a fully straight configuration when no kink-pair can be activated anywhere along its length. The additional applied stress needed to restart wavy glide from the fully arrested straight screw configuration is determined by the weakest region for forming and migrating a kink-pair anywhere along the dislocation line in its new location in the material.

During the intervals of wavy glide, the dislocation configuration is metastable. If the applied stress is removed during free glide, the stress-free equilibrium configuration is severely kinked, appearing to vary in character, not aligned with the original screw orientation. Examples of unloaded dislocation lines from all four planes are shown in Figure 11, along with experimental evidence for tortuous dislocations. According to the PFDD simulations, the more rugged morphology of the {110} and {112} planes compared to the other two planes becomes more pronounced in the stress-free state. Because R in the former planes are lower, kink-pair migration is more difficult, so arrested dislocation lines on these planes contain several edge-segments. With higher R values, kink-pair migration rates are higher,

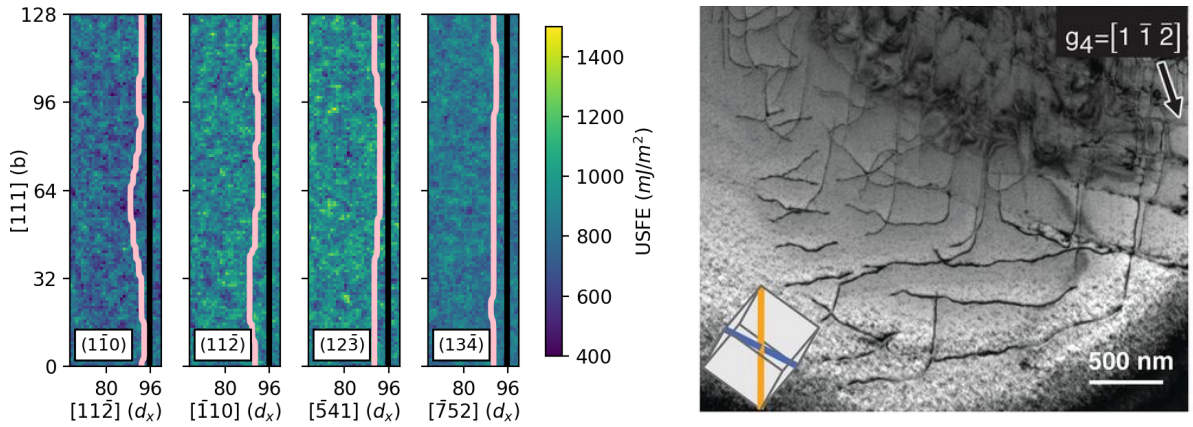

FIG. 11. (Left) Examples of dislocations that were unloaded during glide in PFDD. The black line is the initial dislocation and the pink line is the unloaded dislocation. Just as the dislocations are wavy during glide, they remain wavy under zero stress if the stress is removed. The correlation length l is $1w_0$ for all four cases pictured. (Right) Experimental observations of wavy dislocations in MoNbTi. Taken with permission from [27].

leaving the relaxed lines on the {123} and {134} planes smoother. These wavy dislocations are not unlike those observed experimentally in MoNbTi, where post-mortem investigation revealed wavy, predominantly non-screw, dislocation lines on {110}, {112}, and {123} planes [27].

As kink-pair activation controls the stop/restart behavior, we closely examine the first kink-pair formed for two examples on each slip plane type (Figure 12). The kink-pairs on the top row correspond to the first kink-pair in the lower tail of the σ_i distribution, whereas the bottom row shows examples from the upper tail, i.e., the relatively stronger ones. In all cases, the critical kink-pair begins to form by extending a small "foot" $1b$ in height into a region with a relatively low USFE for formation and immediate migration. Thus, we find that the mechanism to first start motion does not change, only the stress required to activate kink-pairs at the weak areas along the dislocation length. Drawing a parallel to brittle fracture, the stress σ_i to first move the dislocation is governed by the weakest link along the dislocation, wherein the link length is insensitive to l. The broad variation seen in σ_i in all cases would be characteristic of weakest-link behavior. The value of σ_i would consequently be mainly controlled by the lower tail of the USFE, which is similar for all

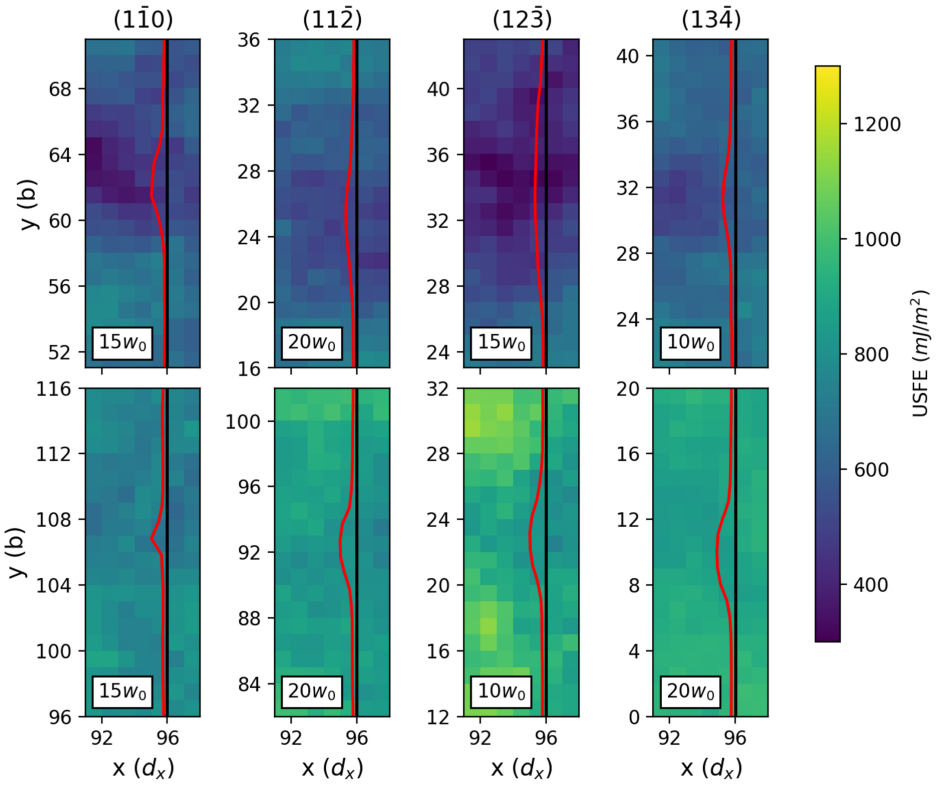

FIG. 12. Examples of kink-pair nucleation on all four slip planes. The kink-pairs in the top row are nucleated on the weakest screw dislocation for their slip plane, while the bottom row shows kink-pairs on the strongest screw dislocation studied. The black line shows the initial placement of the dislocation at zero stress. Regardless of the slip plane, correlation length l, or critical stress, kink-pair nucleation controls the glide behavior of the dislocations.

USFE distributions here, explaining the similarity in the mean value of σ_i among the four slip modes.

Dislocations in all planes glide via this stop/restart mechanism in strain (or time). However, for the {110} plane, dislocations, on average, stop/restart more often in their excursion across the plane than the other planes. Many of the dislocations on the {134} plane are an exception, where in roughly half the cases, $\sigma_i = \sigma_f$. The heterogeneity in lattice energy across the plane increases with the variation in USFE and l. With increased heterogeneity in lattice energy both in space and in magnitude, the dislocation is more likely to encounter a relatively harder location in material in which kink-pair activation is not possible along the entire length of the dislocation, causing it to fully arrest. Thus, for the most heteroge-

neous cases, we see greatest hardening, where the glide resistance increases markedly with glide distance. This explains the increase in the ratio σ_f/σ_i with l for a given plane. To measure the strengthening provided by the heterogeneity, we calculate the hardening ratio, $(\sigma_f - \sigma_i)/\sigma_i$, which is the ratio of the total rise in glide resistance to run the dislocation out of the cell (consistent signature of runaway) divided by the critical stress to first start its motion. Figure 8C confirms the origin of hardening as posed; the strengthening increases with the dispersion (i.e., coefficient of variation) in the USFE.

IV. DISCUSSION

In studying the motion of long screw dislocations gliding over long distances, we show that their glide is controlled by the activation of kink-pair formation and migration. While kink-pair-controlled motion of screw dislocations occurs in pure BCC metals, the kink-pair nucleation frequencies depend on thermal fluctuations and scale with temperature and stress. Temperature introduces random thermal noise, and for a moving dislocation, represents statistical dispersion in driving force. Otherwise, under constant temperature and stress, the probability of forming and migrating kink-pair is the same along the length and invariant with location in the crystal. The dislocation moves by successive single kink-pair activation and straightening. While they are straight and arrested, they lie in waiting for a sufficient thermal perturbation to form and migrate the next kink-pair.

In the present work for an MPEA, the effects of temperature on the stresses to move the dislocation and how the dislocation moves are not included. Specifically, the applied mechanical energy is not supplemented by thermal energy. The chemical composition randomness in the MPEA represents statistical dispersion in the energetic barriers for glide across the plane as opposed to random supply of thermal energy. Thus, the composition variations allow for kink-pairs to form randomly without the randomness from thermal noise. At a non-zero temperature, we would expect that kink-pairs will form more easily in the MPEA than in pure BCC metals because there are both thermal and compositional fluctuations present that can nucleate kink-pairs. Significant numbers of kinks forming on different slip planes can lead to immobile cross-kinks, which have been proposed to play an important role in BCC MPEAs [12, 29].

As in pure metals under temperature and stress, the arrested screw dislocation is nearly

straight and the dislocation waits for sufficient additional energy, in the form of mechanical energy here, to form and migrate a kink-pair or multiple kink-pairs along its length. However, the statistical dispersion in lattice energy introduces periods of wavy travels between arrested states, which does not occur in pure metals. The waviness arises from variable kink-pair activation rates along the same line, leading to different nanoscale segments incurring different amounts of travel. The probability of kink-pair activation is not spatially invariant and depends on the level of heterogeneity in the lattice energy distribution. As another consequence, much of the glide plane slipped by a screw dislocation in an MPEA is accomplished by wavy glide, unlike in a pure metal. In fact, when the MPEA is unloaded, the dislocation collapses to wavy, non-screw state. This could explain prior microscopy studies of deformed refractory MPEAs that show highly kinked rather than straight dislocations [27].

We observe that in all cases of glide planes and correlation lengths, the glide initiates with successful formation and migration of a kink-pair in the weakest region along the length of the dislocation. This activation mechanism will impact the critical stress in several ways. First, initial stresses depend on the lower tail of the lattice energy distribution, not its mean value. Second, the initial stress will be highly position-dependent and can be expected to vary substantially among different but otherwise like dislocations on the same glide plane. Third, since the dislocation cannot advance until the kink-pair migrates, the easier it is for the edge dislocations to move, i.e., the higher the value of R, the lower the initial critical stress. Last, the weakest link type phenomenon engenders a size effect, wherein longer is weaker. In actual materials, the lengths of screw dislocations can be much longer than those studied here ($128b$). The implication is that longer dislocations will experience even more variations along their lengths and even lower activation stresses. These outcomes result from the inherent compositional fluctuations characteristic of MPEAs and can be expected to apply to other MPEA systems as well.

Wavy or jerky dislocation glide is emerging as a common and persistent characteristic of dislocations in MPEAs. Several atomistic or mesoscale modeling simulations and some microscopy studies have reported wavy dislocations in glide or post-mortem [9, 11, 12, 27, 33]. Prior MD studies have associated tortuous morphology of dislocations of any character to randomly occurring pinning points and formation of cross kinks and/or interstitials and vacancies in some nanoscale segments [5, 9, 12, 14]. Similarly, mesoscale models of a generic

dislocation have attributed wavy glide to dislocation bowing out between randomly occurring pinning points [6, 33]. Here in analyzing planar glide behavior of initially screw dislocations, we classify wavy glide and jerky glide as distinct behaviors. Wavy glide is a result of variable rates of kink-pair formation and migration along the length of the dislocation, where nanoscale segments with higher rates extend further. Wavy glide is not directly related to hardening, meaning the activation stress does not change, and any amount of atomic-scale variation in the underlying lattice energy will cause wavy glide. Jerky glide, on the other hand, is a result of the frequent transition between non-stop, free glide with non-zero kink-pair activation rates and complete arrest with zero kink-pair activation rates. Jerky glide means hardening, in which the critical stress increases with strain. We clearly show that the greater the dispersion in lattice energy, the greater the hardening. This glide mechanism, involving wavy morphologies and jerky-induced hardening, is not applicable to initially edge-character dislocations.

Jerky glide and its associated hardening are studied over distances of just $96b$. The hardening seen in stress-strain curves among different dislocations on the same plane type vary substantially as well, such that no two pathways and stress-strain curves are alike. The greater the statistical variation in the USFE, in both content and length scale, the more pronounced the hardening. For the {110} plane, for which we observed the greatest amount of hardening among the four plane types, the critical stress increased, on average, 25–50% from its initial value. In contrast, the {134} plane showed the least. Experimental observations of dislocations in MoNbTi observe dislocations gliding on the {112}, {123}, and {134} planes, with notably fewer dislocations on the {110} planes [27]. In light of the current results, we could interpret this to mean that hardening, rather than the initial critical stress, selects the preferred glide plane. Nevertheless, it can anticipated that if the underlying USFE distribution has large dispersion with a long upper tail (high lattice energy with low probability), then hardening could continue with glide distances greater than the $100b$ simulated here.

Many MD simulations of dislocation glide in the {110} plane of MPEAs attribute the high critical resolved shear stress (CRSS) to the formation of cross-kinks along the same dislocation line [5, 9, 12, 14]. In the present simulations, the driving stress was intentionally applied so that the dislocation glide plane corresponded to the MRSSP of the dislocation; therefore, no driving stress component was applied to drive any part of the dislocation to

cross slip onto another plane. Including thermal effects and/or other applied stress states would promote cross slip, however, the consequences would not necessarily be the same as in a pure metal. As mentioned, in simulating in-plane glide, the motion involves wavy intervals, in which the original screw dislocation adopts a non-screw character, which would not present much opportunity for cross slip. The dislocation nearly recovers its straight screw orientation only when fully arrested under stress, which would then leave the possibility for forming kink-pairs on cross slip planes.

V. CONCLUSIONS

In summary, we employ phase field dislocation dynamics to study the role of screw-to-edge ratio and lattice energy distribution on the morphological transitions and evolution of the critical stresses to move long screw dislocations in the refractory MPEA MoNbTi. The atomic scale fluctuations in elements in MPEAs lead to dislocation-scale heterogeneity in the lattice energies associated with shearing the glide plane. Atomistic calculations find that the screw-to-edge ratios and the mean and dispersion in lattice energy distributions vary among the four plane types in the BCC MPEA MoNbTi, providing the opportunity to study their influence on dislocation dynamics in the same material. We constructed MPEA crystals with over 70 nm long glide planes with these lattice energy distributions and length scales over which the compositions associated with them are correlated. We show that the variation in lattice energy, in both content and scale, lead to a strain hardening-like behavior, a strengthening in the critical stress to activate glide with glide distance. When the variation is large, the dislocation moves in a stop/start motion, alternating between a wavy morphology in free flight and a nearly recovered straight screw orientation in full arrest. Substantial strain hardening behavior is associated with this glide behavior, where the critical stress increases, on average, 20–30% from the stress to first activate motion. In contrast, when the variation is small, the stress to initiate motion most often is the stress for runaway glide, indicating little to no hardening, and the dislocation motion is continually wavy. In all cases,the wavy glide is the result of variable kink-pair formation and migration rates along the dislocation length, where portions with higher rates travel greater distances. The critical stress to move an isolated dislocation in pure metals would not exhibit the strain hardening seen here at the single dislocation scale. The strain hardening induced

by atomic-scale fluctuations in composition in MPEAs could play a part in explaining the superior strengths exhibited by these materials.

VI. ACKNOWLEDGEMENTS

LF acknowledges support from the Department of Energy National Nuclear Security Administration Stewardship Science Graduate Fellowship, which is provided under cooperative agreement number DE-NA0003960. SX and IJB gratefully acknowledge support from the Office of Naval Research under contract ONR BRC Grant N00014-21-1-2536. Use was made of computational facilities purchased with funds from the National Science Foundation (CNS-1725797) and administered by the Center for Scientific Computing (CSC). The CSC is supported by the California NanoSystems Institute and the Materials Research Science and Engineering Center (MRSEC; NSF DMR 1720256) at UC Santa Barbara. AH gratefully acknowledges support from support from the Materials project within the Physics and Engineering Models (PEM) Subprogram element of the Advanced Simulation and Computing (ASC) Program at Los Alamos National Laboratory (LANL). This manuscript has been assigned LA-UR-21-22205.

---

[1] O. N. Senkov, D. B. Miracle, K. J. Chaput, and J. P. Couzinie, Development and exploration of refractory high entropy alloys—A review, J. Mater. Res. **33**, 3092 (2018).

[2] J.-P. Couzinié and G. Dirras, Body-centered cubic high-entropy alloys: From processing to underlying deformation mechanisms, Mater. Charact. **147**, 533 (2018).

[3] Y. Zhang, T. T. Zuo, Z. Tang, M. C. Gao, K. A. Dahmen, P. K. Liaw, and Z. P. Lu, Microstructures and properties of high-entropy alloys, Prog. Mater. Sci. **61**, 1 (2014).

[4] O. Senkov, J.-P. Couzinie, S. Rao, V. Soni, and R. Banerjee, Temperature dependent deformation behavior and strengthening mechanisms in a low density refractory high entropy alloy $Al_{10}Nb_{15}Ta_5Ti_{30}Zr_{40}$, Materialia **9**, 100627 (2020).

[5] S. Rao, C. Varvenne, C. Woodward, T. Parthasarathy, D. Miracle, O. Senkov, and W. Curtin, Atomistic simulations of dislocations in a model BCC multicomponent concentrated solid solution alloy, Acta Mater. **125**, 311 (2017).

[6] L. Zhang, Y. Xiang, J. Han, and D. J. Srolovitz, The effect of randomness on the strength of high-entropy alloys, Acta Mater. **166**, 424 (2019).

[7] M. Sudmanns and J. A. El-Awady, The effect of local chemical ordering on dislocation activity in multi-principle element alloys: A three-dimensional discrete dislocation dynamics study, Acta Materialia **220**, 117307 (2021).

[8] W.-R. Jian, Z. Xie, S. Xu, Y. Su, X. Yao, and I. J. Beyerlein, Effects of lattice distortion and chemical short-range order on the mechanisms of deformation in medium entropy alloy CoCrNi, Acta Mater. **199**, 352 (2020).

[9] B. Chen, S. Li, H. Zong, X. Ding, J. Sun, and E. Ma, Unusual activated processes controlling dislocation motion in body-centered-cubic high-entropy alloys, Proc. Natl. Acad. Sci. **117**, 16199 (2020).

[10] F. Maresca and W. A. Curtin, Mechanistic origin of high strength in refractory BCC high entropy alloys up to 1900 K, Acta Mater. **182**, 235 (2020).

[11] L. T. Smith, Y. Su, S. Xu, A. Hunter, and I. J. Beyerlein, The effect of local chemical ordering on Frank-Read source activation in a refractory multi-principal element alloy, Int. J. Plast. **134**, 102850 (2020).

[12] S. I. Rao, B. Akdim, E. Antillon, C. Woodward, T. A. Parthasarathy, and O. N. Senkov, Modeling solution hardening in BCC refractory complex concentrated alloys: NbTiZr, $Nb_{1.5}TiZr_{0.5}$ and $Nb_{0.5}TiZr_{1.5}$, Acta Mater. **168**, 222 (2019).

[13] R. Pasianot and D. Farkas, Atomistic modeling of dislocations in a random quinary high-entropy alloy, Comput. Mater. Sci. **173**, 109366 (2020).

[14] F. Maresca and W. A. Curtin, Theory of screw dislocation strengthening in random BCC alloys from dilute to "High-Entropy" alloys, Acta Mater. **182**, 144 (2020).

[15] S. Yin, J. Ding, M. Asta, and R. O. Ritchie, Ab initio modeling of the energy landscape for screw dislocations in body-centered cubic high-entropy alloys, npj Comput. Mater. **6**, 110 (2020).

[16] S. Yin, Y. Zuo, A. Abu-Odeh, H. Zheng, X.-G. Li, J. Ding, S. P. Ong, M. Asta, and R. O. Ritchie, Atomistic simulations of dislocation mobility in refractory high-entropy alloys and the effect of chemical short-range order, Nature Comm. **12**, 4873 (2021).

[17] S. Xu, Y. Su, W.-R. Jian, and I. J. Beyerlein, Local slip resistances in equal-molar MoNbTi multi-principal element alloy, Acta Mater. **202**, 68 (2021).

[18] C. D. Statham, D. A. Koss, and J. W. Christian, The thermally activated deformation of niobium-molybdenum and niobium-rhenium alloy single crystals, Philos. Mag. **26**, 1089 (1972).

[19] K. Kang, V. V. Bulatov, and W. Cai, Singular orientations and faceted motion of dislocations in body-centered cubic crystals, Proc. Natl. Acad. Sci. **109**, 15174 (2012).

[20] X. Wang, S. Xu, W.-R. Jian, X.-G. Li, Y. Su, and I. J. Beyerlein, Generalized stacking fault energies and Peierls stresses in refractory body-centered cubic metals from machine learning-based interatomic potentials, Comput. Mater. Sci. **192**, 110364 (2021).

[21] A. Seeger, LXV. On the theory of the low-temperature internal friction peak observed in metals, Philos. Mag. **1**, 651 (1956).

[22] M. S. Duesbery, The influence of core structure on dislocation mobility, Philos. Mag. **19**, 501 (1969).

[23] J. W. Christian, Some surprising features of the plastic deformation of body-centered cubic metals and alloys, Metall. Trans. A **14**, 1237 (1983).

[24] A. Garratt-Reed and G. Taylor, Optical and electron microscopy of niobium crystals deformed below room temperature, Philos. Mag. A **39**, 597 (1979).

[25] Q.-J. Li, H. Sheng, and E. Ma, Strengthening in multi-principal element alloys with local-chemical-order roughened dislocation pathways, Nature Comm. **10**, 3563 (2019), 1904.07681.

[26] D. Caillard, A TEM in situ study of alloying effects in iron. II-Solid solution hardening caused by high concentrations of Si and Cr, Acta Mater. **61**, 2808 (2013).

[27] F. Wang, G. H. Balbus, S. Xu, Y. Su, J. Shin, P. F. Rottmann, K. E. Knipling, J.-C. Stinville, L. H. Mills, O. N. Senkov, I. J. Beyerlein, T. M. Pollock, and D. S. Gianola, Multiplicity of dislocation pathways in a refractory multiprincipal element alloy, Science **370**, 95 (2020).

[28] J. Marian, W. Cai, and V. V. Bulatov, Dynamic transitions from smooth to rough to twinning in dislocation motion, Nature Mater. **3**, 158 (2004).

[29] X. Zhou, S. He, and J. Marian, Cross-kinks control screw dislocation strength in equiatomic bcc refractory alloys, Acta Mater. **211**, 116875 (2021).

[30] G. Dirras, J. Gubicza, A. Heczel, L. Lilensten, J.-P. Couzinié, L. Perrière, I. Guillot, and A. Hocini, Microstructural investigation of plastically deformed $Ti_{20}Zr_{20}Hf_{20}Nb_{20}Ta_{20}$ high entropy alloy by X-ray diffraction and transmission electron microscopy, Materials Charact. **108**, 1 (2015).

[31] D. Hull, J. F. Byron, and F. W. Noble, Orientation dependence of yield in body-centered cubic metals, Can. J. Phys. **45**, 1091 (1967).

[32] A. Seeger and U. Holzwarth, Slip planes and kink properties of screw dislocations in high-purity niobium, Philos. Mag. **86**, 3861 (2006).

[33] Y. Zeng, X. Cai, and M. Koslowski, Effects of the stacking fault energy fluctuations on the strengthening of alloys, Acta Mater. **164**, 1 (2019).

[34] Y. U. Wang, Y. M. Jin, A. M. Cuitiño, and A. G. Khachaturyan, Nanoscale phase field microelasticity theory of dislocations: Model and 3D simulations, Acta Mater. **49**, 1847 (2001).

[35] I. J. Beyerlein and A. Hunter, Understanding nanoscale dislocation mechanics using phase field dislocation dynamics, Philos. Trans. R. Soc. A **374**, 20150166 (2016).

[36] A. Ferrari, B. Dutta, K. Gubaev, Y. Ikeda, P. Srinivasan, B. Grabowski, and F. Körmann, Frontiers in atomistic simulations of high entropy alloys, J. Appl. Phys. **128**, 150901 (2020).

[37] S. Xu, J. Y. Cheng, Z. Li, N. A. Mara, and I. J. Beyerlein, Phase-field modeling of the interactions between an edge dislocation and an array of obstacles, Comput. Methods Appl. Mech. Eng. **389**, 114426 (2022).

[38] M. Koslowski, A. M. Cuitino, and M. Ortiz, A phase-field theory of dislocation dynamics, strain hardening and hysteresis in ductile single crystals, Journal of the Mechanics and Physics of Solids **50**, 2597 (2002).

[39] S. Xu, Y. Su, and I. J. Beyerlein, Modeling dislocations with arbitrary character angle in face-centered cubic transition metals using the phase-field dislocation dynamics method with full anisotropic elasticity, Mech. Mater. **139**, 103200 (2019).

[40] V. Vitek, Intrinsic stacking faults in body-centred cubic crystals, Philos. Mag. **18**, 773 (1968).

[41] L. Yang, P. Söderlind, and J. A. Moriarty, Accurate atomistic simulation of $(a/2)\langle 111\rangle$ screw dislocations and other defects in bcc tantalum, Philos. Mag. A **81**, 1355 (2001).

[42] S. L. Frederiksen and K. W. Jacobsen, Density functional theory studies of screw dislocation core structures in bcc metals, Philos. Mag. **83**, 365 (2003).

[43] X. Zhang, J. Tang, L. Deng, G. Zhong, X. Liu, Y. Li, H. Deng, and W. Hu, The effects of interstitial impurities on the mechanical properties of vanadium alloys: a first-principles study, J. Alloys Compd. **701**, 975 (2017).

[44] C. Yang and L. Qi, Modified embedded-atom method potential of niobium for studies on mechanical properties, Comput. Mater. Sci. **161**, 351 (2019).

[45] L. Dezerald, L. Proville, L. Ventelon, F. Willaime, and D. Rodney, First-principle prediction of kink-pair activation enthalpy on screw dislocations in bcc transition metals: V, Nb, Ta, Mo, W, and Fe, Phys. Rev. B **91**, 094105 (2015).

[46] S. Xu, Y. Su, L. T. W. Smith, and I. J. Beyerlein, Frank-Read source operation in six body-centered cubic refractory metals, J. Mech. Phys. Solids **141**, 104017 (2020).

[47] S. Xu, J. R. Mianroodi, A. Hunter, B. Svendsen, and I. J. Beyerlein, Comparative modeling of the disregistry and Peierls stress for dissociated edge and screw dislocations in Al, Int. J. Plast. **129**, 102689 (2020).

[48] S. Xu, E. Hwang, W.-R. Jian, Y. Su, and I. J. Beyerlein, Atomistic calculations of the generalized stacking fault energies in two refractory multi-principal element alloys, Intermetallics **124**, 106844 (2020).

[49] S. Xu, S. Z. Chavoshi, and Y. Su, On calculations of basic structural parameters in multi-principal element alloys using small atomistic models, Comput. Mater. Sci. **202**, 110942 (2022).

[50] R. A. Romero, S. Xu, W.-R. Jian, I. J. Beyerlein, and C. Ramana, Atomistic simulations of the local slip resistances in four refractory multi-principal element alloys, Int. J. Plast. **149**, 103157 (2022).

[51] S. I. Rao, E. Antillon, C. Woodward, B. Akdim, T. A. Parthasarathy, and O. N. Senkov, Solution hardening in body-centered cubic quaternary alloys interpreted using Suzuki's kink-solute interaction model, Scr. Mater. **165**, 103 (2019).

[52] A. Ghafarollahi, F. Maresca, and W. A. Curtin, Solute/screw dislocation interaction energy parameter for strengthening in bcc dilute to high entropy alloys, Model. Simul. Mater. Sci. Eng. **27**, 085011 (2019).

[53] Y. Z. Hu and K. Tonder, Simulation of 3-D random rough surface by 2-D digital filter and fourier analysis, Int. J. Mach. Tools Manuf. **32**, 83 (1992).

[54] M. Duesberry, V. Vitek, and D. Bowen, The effect of shear stress on the screw dislocation core structure in body-centred cubic lattices, Proc. R. Soc. Lond. A **332**, 85 (1973).

[55] B. Joos and M. Duesbery, The peierls stress of dislocations: an analytic formula, Physical Review Letters **78**, 266 (1997).

[56] F. Mompiou, D. Tingaud, Y. Chang, B. Gault, and G. Dirras, Conventional vs harmonic-structured β-Ti-25Nb-25Zr alloys: A comparative study of deformation mechanisms, Acta Mater. **161**, 420 (2018).

[57] F. G. Coury, M. Kaufman, and A. J. Clarke, Solid-solution strengthening in refractory high entropy alloys, Acta Mater. **175**, 66 (2019).

[58] V. Vitek, Structure of dislocation cores in metallic materials and its impact on their plastic behaviour, Prog. Mater. Sci. **36**, 1 (1992).